Catalysis Today 154 (2010) 195–201

Contents lists available at ScienceDirect

Catalysis Today

journal homepage: www.elsevier.com/locate/cattod

Deactivation of Pt/MnO_x–CeO_2 catalysts for the catalytic wet oxidation of phenol: Formation of carbonaceous deposits and leaching of manganese

R. Kouraichi [a], J.J. Delgado [a,*], J.D. López-Castro [a], M.Stitou [b], J.M. Rodríguez-Izquierdo [a], M.A. Cauqui [a,**]

[a] Universidad de Cádiz, Departamento de Ciencia de los Materiales e Ingeniería Metalúrgica y Química Inorgánica, Facultad de Ciencias, 11510-Puerto Real (Cádiz), Spain
[b] University Abdelmalek Essaâdi, Faculty of Sciences of Tétouan, Morocco

ARTICLE INFO

Article history:
Available online 23 May 2010

Keywords:
Catalytic wet oxidation
Phenol
Cerium
Manganese
Platinum catalyst
Deactivation

ABSTRACT

MnO_x–CeO_2 and Pt(2%)/MnO_x–CeO_2 catalysts were prepared and investigated in the catalytic wet oxidation (CWO) of phenol. The reaction was carried out in a high-pressure autoclave reactor operating at 140 °C and oxygen partial pressure of 2 MPa. The effect of a reduction pre-treatment at 350 °C on the catalytic performance of both, the platinum catalyst and the bare oxide was studied. Higher activities were found for the reduced catalysts, independently of the presence or absence of Pt. Formation of carbonaceous deposits on the catalytic surface and leaching of manganese was confirmed as the two major deactivation mechanisms occurring in CWO of phenol. The amounts of deposits formed and manganese leached were higher in the case of reduced samples. Different techniques (XRD, HREM, HAADF, EDS, ICP) were used to characterise the chemical and structural changes experimented by the catalysts during reaction. The behaviour of reduced catalysts was found to be associated to the presence of MnO. The formation of this manganese oxide phase during the reduction pre-treatment significantly influenced the catalytic performance and stability of the catalysts under operation conditions.

1. Introduction

A significant amount of papers dealing with environmental pollution control has highlighted the catalytic wet oxidation (CWO) technique as an efficient and technologically viable method to remove organic pollutants from wastewaters [1,2]. Phenol is chosen as a model contaminant in most of these studies, because it is a very common raw material extensively used in dye, petrochemical and pharmaceutical industries, among others. On the other hand, the use of heterogeneous solid catalysts in wet oxidation is preferred as they are easily recoverable and eventually reusable. More specifically, MnO_x–CeO_2 oxides have been widely used for CWO of aqueous phenolic solutions, showing a remarkable activity for phenol removal from liquid solutions [3,4].

Although the notable catalytic performance of the MnO_x–CeO_2 composites, they exhibit important deactivation problems [5]. The formation of carbonaceous deposits has been considered as the major cause for the activity loss. Previous studies on CWO of phenol [6,7] over MnO_x–CeO_2 catalyst revealed that, even when complete removal of organic carbon from the solution was achieved, an important part of the initial amount of carbon was transformed into a polymeric material vigorously adsorbed on the catalyst surface, leading to the catalyst deactivation via a physical blockage of the active sites. Delgado et al. [8] reported the formation of a C-layer of about 20 nm on the catalyst surface, when operating CWO of phenol at low temperature and moderate oxygen partial pressure. Promotion of MnO_x–CeO_2 with noble metals, especially with platinum, may help to inhibit the polymerization side reactions, thus reducing the formation of carbonaceous deposits and prolonging the catalyst longevity [9,10]. However, it was recently found that platinum catalysts may suffer rapid loss of activity, which is mainly attributed to either poisoning by surface impurities, or deactivation due to high oxygen coverage (over-oxidation) [11].

In the case of manganese based catalysts, the leaching of active phase is also an undesirable effect, not only due to its contribution to the activity loss, but also because the presence of manganese cations in the aqueous effluent can be considered as highly toxic to marine life [12].

The menace of catalyst deactivation may seriously compromise the success of industrial application of CWO technology. In this sense, a better understanding of factors influencing the appearance of these mechanisms is needed, in order to properly design active and stable catalysts more resistant to deactivation.

In this paper we investigate the behaviour of a series of MnO_x–CeO_2 and Pt/MnO_x–CeO_2 catalysts for the catalytic wet oxidation of phenol. The influence of the reduction treatment used to

* Corresponding author. Tel.: +34 956016341.
** Corresponding author.
E-mail addresses: juanjose.delgado@uca.es (J.J. Delgado), miguelangel.cauqui@uca.es (M.A. Cauqui).

0920-5861/$ – see front matter © 2010 Elsevier B.V. All rights reserved.
doi:10.1016/j.cattod.2010.04.020

activate the catalysts on the global catalytic performance has been addressed. We pay special attention to the stability of the catalysts under reaction conditions, by making an in depth characterisation of both, fresh and used samples. For this purpose, a wide battery of techniques as XRD, TEM, HAADF-STEM, EELS, X-EDS were used. In particular, the evolution of manganese oxide is monitored, and its changes in composition, morphology and structure discussed in terms of the catalytic activity and selectivity, the stability against leaching under reaction conditions, and the formation of carbonaceous deposits. The results derived from this study allow us to establish a correlation between catalytic performance, including deactivation resistance, and chemical and structural properties of the catalysts.

2. Experimental

2.1. Materials

Cerium nitrate $Ce(NO_3)_3{\cdot}6H_2O$ (99.5%), ammonium oxalate $(NH_4)_2C_2O_4{\cdot}H_2O$ (99–101%) and hydroxide solution of tetraaminplatinum (II) $[Pt(NH_3)_4](OH)_2$ from Alfa Aesar (Johnson Matthey) and manganese nitrate $Mn(NO_3)_2{\cdot}4H_2O$ (>98.5%) from Merck Chemicals were used for the synthesis of catalysts. Phenol crystallized (99.5%) from Panreac was used without further purification. Other organic materials (2, 6-dimethylphenol PESTANOL (99.9%), phenol standard (99.9%) and volatile free acid standard mix) used in GC analyses were from Sigma Aldrich. Oxygen gas of 99.9% purity was used in the oxidation reaction.

2.2. Catalyst preparation

MnO_x–CeO_2 oxide (Mn/(Mn + Ce) = 0.5, molar ratio) was prepared by the co-precipitation method. Typically, a mixture of cerium nitrate and manganese nitrate was added slowly to a solution of 0.2 M ammonium oxalate under stirring. After filtration and washing with oxalic acid (0.01 M) and water, the as-prepared solid was dried at 80 °C for a few days and further calcined at 500 °C for 3 h in a muffle furnace.

Pt/MnO_x–CeO_2 catalyst with platinum loading of 2 wt.% was prepared via incipient wetness impregnation. Subsequently, the Pt catalyst was calcined at 500 °C for 1 h to guarantee a common well-defined starting redox state.

The reduction treatments applied to the support and Pt-loaded catalyst were done in a flow of H_2(5%)/Ar (60 STP cm^3/min) at a heating rate of 5 °C/min. The catalysts were held for 2 h at 350 °C, evacuated at 400 °C for 1 h, cooled under flowing He and further passivated at room temperature under flowing O_2 (5%)/He. The reduced samples are named as MnO_x–CeO_2 R350 and Pt/MnO_x–CeO_2 R350, respectively, to differentiate from non-reduced catalyst.

2.3. Catalyst characterization

Chemical compositions of the samples were obtained by using inductively coupled plasma-atomic emission spectrometry (ICP-AES), in a Plasma Iris Intrepid spectrometer. This technique was also used to investigate the leaching of active phase.

The XRD patterns were obtained on a D8Advance (Bruker AXS) diffractometer, with Cu Kα radiation (λ = 1.5406 Å), a scan step of 0.02° and a step time of 3 s. Transmission Electron Microscopy (TEM) measurements were performed on a JEOL2010F instrument, with 0.19 nm spatial resolution at Scherzer defocus conditions. High Angle Annular Dark Field-Scanning Transmission Electron Microscopy (HAADF-STEM) images were recorded on the same microscope by using an electron probe of 0.5 nm of diameter and a diffraction camera length of 10 cm. The use of STEM mode in combination with X-EDS detectors (Oxford Instrument) allows the possibility to perform chemical analysis with a spatial resolution better than 1 nm.

Surface area (S_{BET}) values were obtained from the nitrogen adsorption/desorption isotherms at 77 K, using a fully automated model ASAP 2020 gas adsorption system (Micromeritics Instruments). The pore-size analysis has been obtained by applying the BJH method [13].

The reducibility of the catalysts was investigated by temperature-programmed reduction (TPR), using a quadrupole mass spectrometer (Pfeiffer Vacuum Balzers, model QMS 200) equipped with a single Faraday detector, and controlled via a computer using the software Quadstar 422. Typically, 100 mg of sample were loaded in a U-shaped quartz microreactor and treated during 1 h with He at 350 °C, to remove water adsorbed on the sample surface. After cooling down to room temperature, the reduction gas (5% H_2/Ar) was introduced at a flow rate of 60 STP cm^3/min. The system was stabilized for 2 h, and then the temperature programmed to heat with a ramp of 10 °C/min up to 950 °C.

The carbon content of the carbonaceous deposits accumulated on the catalyst surface during the oxidation of phenol was quantified by CHN elemental analysis, using a CHNS-932 equipment of LECO Corporation.

2.4. Reaction procedure and analytical methods

Catalytic wet air oxidation reactions were carried out in a 0.5 l autoclave reactor equipped with a pollutant injector, a valve for sampling, a pressure gauge and a magnetically driven stirrer. To optimize the oxygen dissolution and to permit the maximal contact between the reactants and the catalytic powder dispersed in solution, the stirring rate of the turbine was set at 800 rpm. Reactions were run at 140 °C, under O_2 partial pressure of 2 MPa (total pressure of 3.5 MPa ($N_2 + O_2$)). The autoclave was first charged with 250 ml of distillated water and 1 g of catalyst powder, and then heated up to the reaction temperature. Once the system had stabilized at the desired reaction conditions, 10 ml of a solution containing phenol ([Phenol] = 65,000 ppm) were injected to obtain a final phenol concentration of 2500 ppm. This point was taken as "zero time". Two aliquots of liquid (3.5 ml) were periodically withdrawn. Only the second aliquot was filtered and analyzed, since the first one was used to purge the sampling line.

The total organic carbon (TOC) in solution, expressed in milligrams of carbon per liter, was measured with a Shimazdu 5050 TOC analyzer. The residual phenol concentration was determined using a gas chromatograph (GC 8000 ^{Top}, CE Instruments) equipped with a detector of flame ionization (Model FID-80). The volume of sample injected was 2 μl. A NUKOL^{TM} Supelco (30 m × 0.53 mm × 0.5 μm film thickness) capillary column was used in a temperature-programmed mode. 2,6-Dimethylphenol was used as internal standard.

Data from overall carbon balances were used to calculated product selectivity to CO_2 (S_{CO_2}), carbonaceous deposit (S_d) and soluble intermediates (S_s). The calculations were made as follows:

$$S_{CO_2} = \frac{C_o - C_d - C_{TOC}}{C_O - C_P} \times 100 \quad (1)$$

$$S_d = \frac{C_d}{C_O - C_P} \times 100 \quad (2)$$

$$S_S = \frac{C_{TOC} - C_P}{C_O - C_P} \times 100 \quad (3)$$

where C_O is the initial concentration of phenol, and C_P and C_{TOC} are, respectively, the residual phenol and the total organic carbon concentrations after reaction, all of them expressed in ppm of carbon.

Table 1
Chemical analysis and textural properties of fresh catalysts.

Catalyst	ICP			BET analysis		
	Ce (% molar)	Mn (% molar)	Pt (wt.%)	Surface area (m^2/g)	Pore volume (cm^3/g)	Average pore diameter (Å)
MnO_x–CeO_2	53.3 ± 2.0	46.7 ± 1.0	–	47	0.089	55
MnO_x–CeO_2 R35	–	–	–	46	0.091	59
Pt/MnO_x–CeO_2	56.3 ± 1.4	43.7 ± 1.0	1.8 ± 0.1	43	0.080	55
Pt/MnO_x–CeO_2 R35	–	–	–	40	0.084	60

C_d is the total amount of carbon removed from the solution and converted in carbonaceous deposit, i.e. the TOC abatement due to this process, and it is calculated from CNH elemental analysis of the samples collected after reaction.

3. Results and discussion

3.1. Characterization of fresh catalysts

Table 1 summarizes the chemical composition and textural properties of MnO_x–CeO_2 and Pt/MnO_x–CeO_2 catalysts. As shown, similar values of BET surface area, pore volume and pore size were observed for promoted and unpromoted oxides. These values remained practically unchanged after reduction at 350 °C.

Fig. 1 shows the XRD patterns obtained for the catalysts. All these patterns are dominated by sharp and intensive diffraction peaks corresponding to cubic fluorite-type CeO_2 structure (JCPDS 43-1002). Separated MnO_x peaks of very low intensity were also observed. In the case of MnO_x–CeO_2 oxide (Fig. 1D), theses additional peaks, appearing around 32.5°, 36° and 60°, may be attributed to Mn_3O_4 with hausmannite structure (JCPDS 24-0734). These peaks were not present in the pattern obtained for Pt/MnO_x–CeO_2 (Fig. 1B). However, in this latter pattern we can see how the intensities ratio for peaks at 28.5° and 33° is lower than expected for pure ceria, which can be interpreted as due to an additional contribution in the intensity at $2\theta = 33°$ by the presence of α-Mn_2O_3 (diffraction line for this oxide also at 33°, JCPDS 24-0508). Small peaks at 23° and 55° may corroborate this assignation. In the case of reduced catalysts (Fig. 1A and C), diffraction peaks corresponding to MnO (JCPDS 75-0626) were clearly evidenced in the XRD patterns. Oxides with manganese in higher oxidation states were not detected by XRD after treatment with H_2 at 350 °C. On the other hand, the absence of additional peaks characteristic of Pt in Fig. 1A and B suggests that this metal was well dispersed on the oxide surface, either as Pt^0 or likely forming PtO_x, in the case of the non-reduced Pt/$MnO_x CeO_2$ catalyst.

The reducibility of MnO_x–CeO_2 and Pt/MnO_x–CeO_2 catalysts was investigated by means of the TPR technique, following the evolution of water formed under flowing H_2(5%)/Ar as a function of temperature. The reduction profiles are shown in Fig. 2. As can be seen in this figure, a common high temperature feature centred at ca. 800 °C was always present, which has been associated to bulk reduction of ceria [14,15]. It should be pointed out that the position of this peak did not seem to be modified by the presence of MnO_x or Pt. The TPR profile of MnO_x–CeO_2 (Fig. 2D) also shows two overlapped reduction peaks, with maxima at 450–500 °C, and a slight shoulder at ca. 320 °C. These peaks can be attributed to reduction of

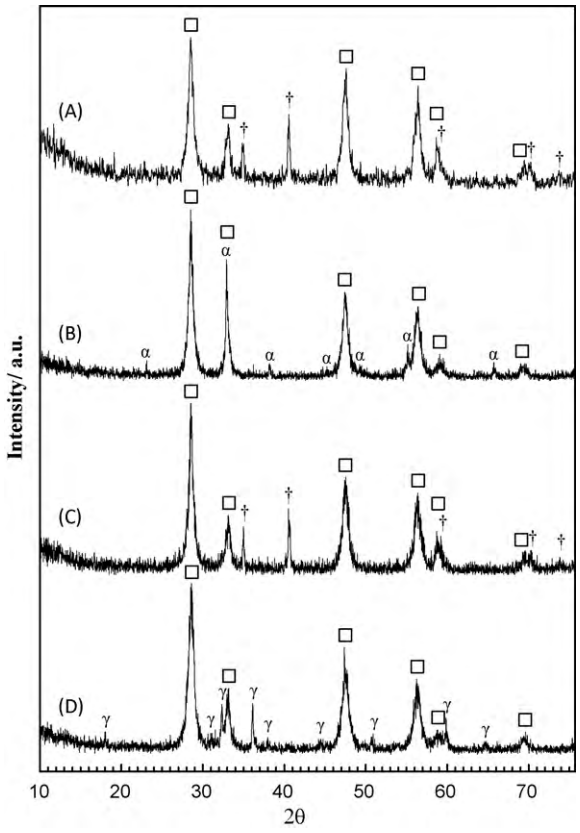

Fig. 1. XRD patterns of (A) Pt/MnO_x–CeO_2 R35; (B) Pt/MnO_x–CeO_2; (C) MnO_x–CeO_2 R35 and (D) MnO_x–CeO_2. The symbols correspond to CeO_2 (□), α-Mn_2O_3 (α), MnO (†) and γ-Mn_3O_4 (γ).

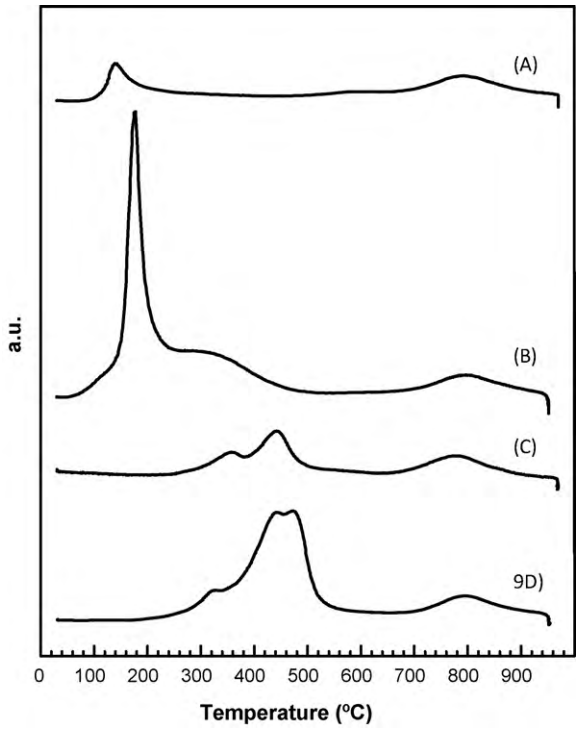

Fig. 2. TPR-H_2O traces (m/e 18) corresponding to (A) Pt/MnO_x–CeO_2 R35; (B) Pt/MnO_x–CeO_2; (C) MnO_x–CeO_2 R35 and (D) MnO_x–CeO_2.

Mn oxides (Mn_2O_3, $Mn_3O_4 \rightarrow MnO$) [16], and also to surface reduction of ceria, this latter normally occurring in the range 500–550 °C [14]. As deduced from Fig. 2B, the peaks assigned to MnO_x and surface ceria reduction processes were almost completely lacking in the presence of platinum. By contrast, this profile shows some new features at lower temperatures (100–350 °C), generally attributed to noble metal reduction, as well as to an enhancement of MnO_x and CeO_2 reducibility in the presence of the noble metal due to the spillover of hydrogen from the Pt to the support [14]. In the cases of pre-reduced MnO_x–CeO_2 and Pt/MnO_x–CeO_2 catalysts (Fig. 2A and C), the intensity of peaks is much lower, and their appearance would be associated to non-fully reduced (after treatment with H_2 at 350 °C) or reoxidased (during passivation and further storage of the samples) Mn and Ce oxides.

According to the interpretation of TPR diagrams, we can conclude that the redox starting points of both, noble metal and support, were rather different for reduced and non-reduced catalysts, thus corroborating the results obtained by XRD. The analysis of the catalytic performance obtained for this series of samples will bring important information about the effect of the initial oxidation state of the manganese on the CWO activity. This effect is frequently ignored in the literature when comparing catalytic behaviours of promoted and unpromoted oxides, and it may provoke and important error in the interpretation of promotion effect, mainly when the chemical and structural properties of these oxides are sensitive to the treatments used to activate the noble metal.

The strong segregation of phases suggested by XRD was confirmed by TEM and EDS measurements. Fig. 3A–C shows HREM images, registered at different magnification, and all of them representative of the fresh catalysts. The low magnification image included in Fig. 3A illustrates the general aspect of the MnO_x–CeO_2 oxide. With respect to size and chemical composition, two different types of particles could be distinguished. On one hand, we observed the presence of large particles (>50 nm), identified by EDS analysis as Ce-free manganese oxides (type I crystallites). On the other hand, small crystals (<7 nm) of a Ce–Mn oxide solid solution were also present in the sample (type II crystallites). The cerium/manganese molar ratio measured in the solid solution crystals was close to 85:15, which is in good agreement with the segregation of pure manganese oxide (type I) crystallites. The formation of fluorite-structured cubic solid solution with MnO_x and CeO_2 oxides has been previously reported [17]. However, the solubility of manganese into the CeO_2 lattice is relatively small, due to the differences in the ionic radius of Mn^{4+} (or Mn^{3+}) and Ce^{4+}. Structural details of type II crystallites are shown in Fig. 3B. It is important to note that MnO_x nanoparticles normally appear surrounded by type II crystallites, as illustrated in Fig. 3C, thus suggesting the occurrence of a strong interaction between these two oxides, which is frequently proposed in the literature as the origin of the synergetic effect accounting for the excellent behaviour of Mn–Ce oxide composites in wet oxidation processes [18,19]. According to these authors, the synergetic mechanism can be essentially regarded as the activation of molecular oxygen by the active sites on MnO_x through CeO_2 (or Ce–Mn solid solution), this latter phase thus acting as oxygen reservoir. From the particles interaction suggested by Fig. 3C, we can conclude that not only manganese sites of the Ce–Mn solid solution (type II crystallites), but also those located on pure MnO_x (type I) could benefit from the redox properties of ceria.

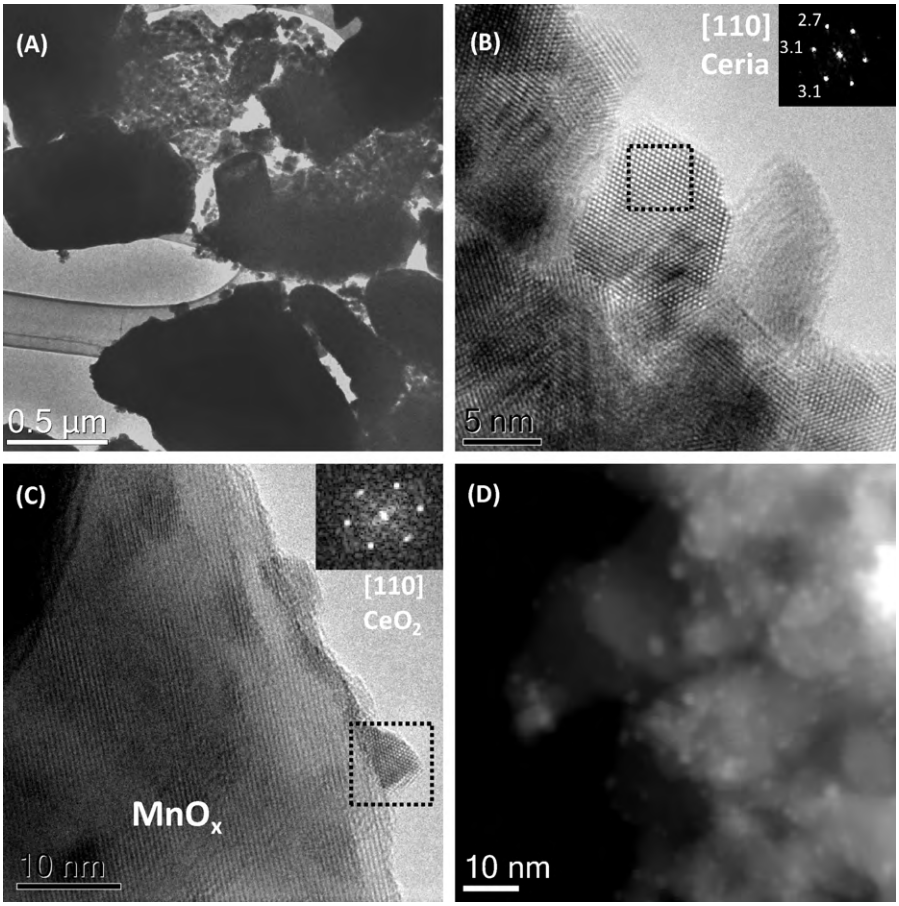

Fig. 3. (A–C) HREM images of the initial MnO_x–CeO_2 oxide and (D) HAADF image of the fresh Pt/MnO_x–CeO_2 R350 catalyst. Digital diffraction pattern of selected areas are included in the inset.

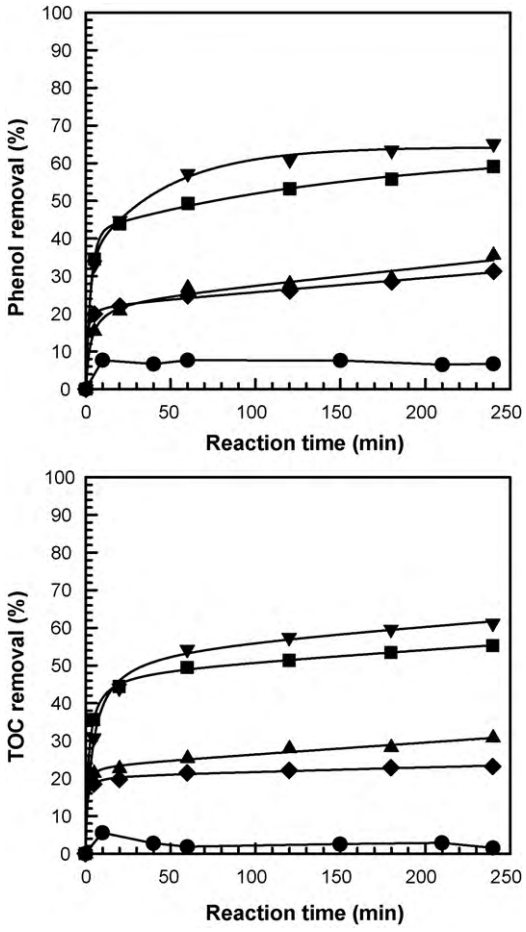

Fig. 4. Phenol (top) and TOC (bottom) removal during CWO over Pt/MnO_x–CeO_2 R35 (■); Pt/MnO_x–CeO_2 (♦); MnO_x–CeO_2 R35 (▼) and MnO_x–CeO_2 (▲) samples. A blank experiment without catalyst is also included (●).

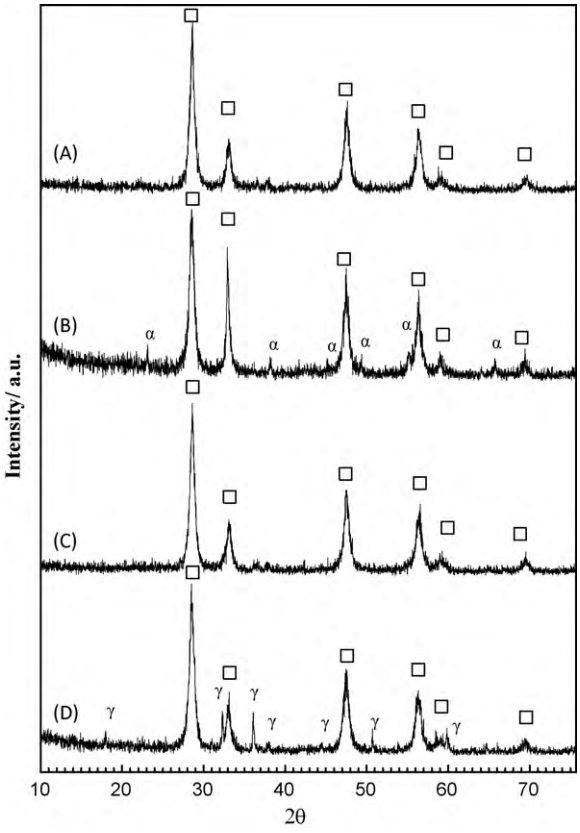

Fig. 5. XRD patterns of (A) MnO_x–CeO_2 R35; (B) MnO_x–CeO_2; (C) Pt/MnO_x–CeO_2 R35 and (D) Pt/MnO_x–CeO_2 after reaction. CeO_2 (□), α-Mn_2O_3 (α) and γ-Mn_3O_4 (γ).

Fig. 3D shows an HAADF image corresponding to the Pt/MnO_x–CeO_2 R35 catalyst. The higher atomic number of platinum in comparison with the support allowed us to distinguish (as bright contrasts) the presence of small Pt particles. The nature of these particles was confirmed by using elemental microanalysis (X-EDS). Values of 1.8 nm for the mean particle size, and 67% for Pt dispersion were obtained. According to TEM images, no significant changes in the morphology of MnO_x–CeO_2 particles were observed after reduction.

3.2. Catalytic wet oxidation of phenol over MnO_x–CeO_2 and Pt/MnO_x–CeO_2

Fig. 4 shows the catalytic activity of the samples for the wet oxidation of phenol at 140 °C and O_2 partial pressure of 2 MPa. As observed in this figure, all the catalysts exhibited a similar profile characterized by an initial period with high activity followed by total activity decay. Only a very small amount of acetic acid was identified as intermediate, thus accounting for the similar conversion values obtained for a given catalyst in terms of both, phenol and TOC removal. Deactivation was confirmed by submitting the catalysts to a second consecutive run. Conversion profile for the second run was always similar to the one obtained for the non-catalytic reaction (blank experiment). As seen in Fig. 4, the catalytic activities of the reduced samples were double the ones obtained for non-reduced catalysts. Moreover, and also worth of noting, the addition of platinum did not improve the conversion values obtained with the bare oxides, irrespectively of the treatment used to activate the noble metal. Regarding the phenol (or TOC) conversion values, the effect of the metal was therefore negligible in comparison with the effect of the activation treatment (oxidative or reductive) to which the catalysts were submitted. As indicated in Section 3.1, the reduction treatment at 350 °C clearly modified the oxidation state of Mn, which appeared after reduction predominantly as Mn^{2+} (MnO). This fact is apparently in contradiction with a well accepted assumption which attributes the excellent CWO performance of MnO_x-based catalysts to the presence of manganese ions in higher oxidation states (Mn^{4+}, Mn^{3+}) [20].

In order to evaluate the real phenol mineralization, different product selectivities were calculated from data obtained in the final carbon balance (Table 2). The reduced catalysts (Pt/MnO_x–CeO_2 R35

Table 2
Phenol conversion and selectivities to CO_2 (S_{CO_2}), carbonaceous deposits (S_d), and soluble intermediates (S_s), corresponding to catalytic tests plotted in Fig. 4. Values for leaching of Mn and S_{BET} of the catalyst after reaction are also included.

Catalyst	Phenol conversion (%)	S_d (%)	S_s[a] (%)	S_{CO_2} (%)	% Mn dissolved	Surface area (m^2/g)
MnO_x–CeO_2	35.5	61.9	13.3	24.8	4.68	1.5
MnO_x–CeO_2 R35	65.1	65.1	6.0	28.9	10.27	3.6
Pt/MnO_x–CeO_2	31.2	55.5	25.8	18.7	1.35	1.4
Pt/MnO_x–CeO_2 R35	59.1	56.3	6.5	37.2	4.47	2.3

[a] Mainly as acetic acid.

and MnO_x–CeO_2 R35) exhibited higher phenol conversion and also better performance toward complete mineralization of phenol (in terms of CO_2 selectivity). It is remarkable that, despite the presence of noble metal, likely as PtO_x, the non-reduced $Pt/CeMnO_x$ catalyst showed the lowest CO_2 selectivity, mainly due to the high concentration of intermediates formed in this case. As observed in Table 2, a large amount of the phenol converted was transformed into carbonaceous deposits, the selectivity to this undesirable product being in the range from 55 to 65%. Values for surface area of used catalysts are also included in this table. In comparison with the values obtained for the fresh catalysts, a dramatic decrease of surface area, as a consequence of carbon deposition, was observed. The blocking of the catalytic surface may be then confirmed as a major cause for the deactivation occurring in CWO of phenol over MnO_x–CeO_2 and Pt/MnO_x–CeO_2 catalysts.

As indicated in Table 2, significant values of leached manganese were found after reaction; the highest value (10%) obtained for the MnO_x–CeO_2 R35 catalyst. The amounts of manganese leached were lower in the case of platinum catalysts, thus suggesting a stabilization of Mn by the presence of the noble metal. In both series, Pt-promoted and unpromoted MnO_x–CeO_2 oxides, the leaching increases with phenol conversion and CO_2 selectivity.

3.3. Characterization of spent catalysts

Fig. 5 shows the XRD patterns obtained for recovered (spent) catalysts. The major difference between these patterns and the ones obtained for the fresh samples is the absence of peaks corresponding to manganese oxides for both, MnO_x–CeO_2 R35 and Pt/MnO_x–CeO_2 R35 spent catalysts. The Mn/Ce molar ratios of these samples, measured by ICP, were 0.72 and 0.76, respectively, thus ruling out the possibility of a total loss of manganese from the solids during reaction. The changes in XRD patterns might be explained in terms of a morphological and/or structural modification of MnO particles towards a less crystalline phase which escaped from X-ray detection. On the contrary, no modifications with respect to fresh states were observed in the case of non-reduced MnO_x–CeO_2 and Pt/MnO_x–CeO_2 catalysts, thus indicating a higher structural stability of these samples.

The spent catalysts were also investigated by TEM, to get more insight into the morphological and structural changes occurred during reactions. Fig. 6A shows a representative HREM image of a deactivated catalyst, in which we observe ceria particles totally surrounded by an amorphous layer of carbonaceous deposit. These deposits were also identified surrounding MnO_x and Pt particles, as illustrated in Fig. 6B. In addition to this carbonaceous layer, the analysis of images obtained for reduced catalysts after reaction revealed the formation of a new type of nanorod-like particles (Fig. 6C and D), instead of the big MnO_x crystals observed in the fresh samples. These MnO_x nanorods showed a quite uneven surface at the ends (Fig. 6D), as resulting from a chemical attack during reaction. Also worth of noting, the elemental analysis of carbonaceous deposits performed by EDS revealed the presence of manganese, thus indicating that a part of the leached manganese remained trapped on this layer.

This ensemble of results may be interpreted in terms of a deactivation process for the wet oxidation of phenol over MnO_x–CeO_2 based catalysts consisting of: (a) the formation of a carbonaceous deposit and (b) the partial dissolution of manganese. The occurrence of these two mechanisms has been clearly evidenced by

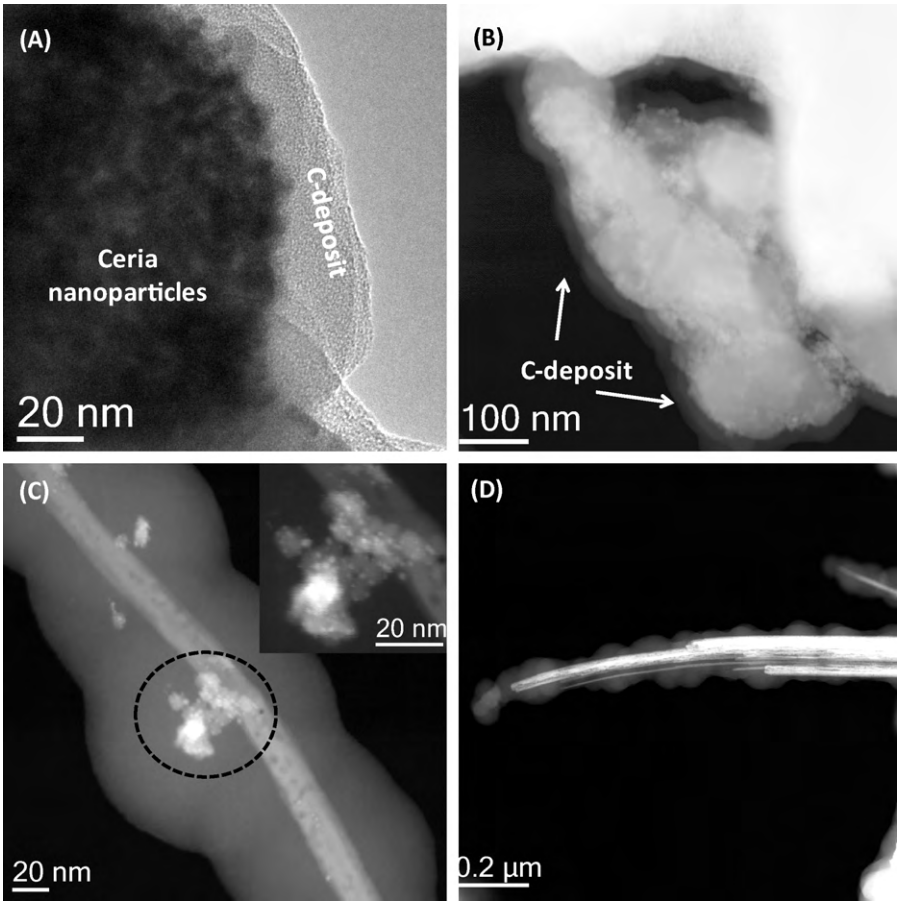

Fig. 6. (A) HREM and (B) HAADF images of Pt/MnO_x–CeO_2 (after reaction) and (C and D) HAADF images of Pt/MnO_x–CeO_2 R35 (after reaction).

TEM. The leaching of active phase was especially significant when manganese oxide was present as MnO (reduced catalysts). In such cases, the dissolution of manganese ions occurred simultaneously with a morphological/structural transformation from big MnO crystals to small MnO_x nanorod-like particles. The identification of manganese atoms trapped on the carbonaceous deposits might suggest the simultaneous and rapid occurrence of the two mentioned deactivation mechanisms. In the case of reduced catalysts, the structural and morphological changes affecting MnO provoke the rate for carbonaceous layer deposition to slow down, thus improving the catalytic performance observed for these samples.

4. Conclusions

The catalytic wet oxidation of phenol was investigated in the presence of MnO_x–CeO_2 and Pt/MnO_x–CeO_2 catalysts. The catalysts were activated by calcination at 500 °C, and also by calcination followed by a further reduction treatment in H_2(5%)/Ar at 350 °C. The characterisation of fresh catalysts by means of TEM techniques confirmed the structural complexity of Mn/Ce oxides. By using XRD diffraction, it was found that after reduction treatment, the manganese oxide was mainly forming big MnO particles. The reduced MnO_x–CeO_2 and Pt/MnO_x–CeO_2 catalysts showed the higher activities in terms of phenol (or TOC) conversion and also the higher selectivities to CO_2 (mineralization). According to phenol degradation profiles, the catalysts deactivated very rapidly, almost immediately after the start of the runs. Formation of carbonaceous deposits and leaching of manganese were identified and proved as mechanisms for such deactivation. The leaching of manganese was lower in the case of platinum catalysts, thus suggesting a stabilization of Mn by the presence of the noble metal. The non-reduced catalysts were found to be morphological and structurally stable during reaction. In these catalysts, manganese is mainly forming Mn_2O_3 or Mn_3O_4 oxides. On the contrary, in the case of reduced samples, a significant transformation of big MnO crystals into nanorod MnO_x particles was proved with the help of Transmission Electron Microscopy technique under HREM and HAADF modes. The higher amount of leaching found for reduced catalysts could be also associated to the poor stability of MnO under acidic reaction conditions. The structural changes affecting MnO particles might prevent the formation of carbonaceous deposits during the first minutes of reaction, thus explaining the higher mineralization of phenol obtained with reduced catalysts.

Acknowledgement

Authors thank financial support from MICIIN-Spain/FEDER-EU (Project MAT2008-00889-NAN) and MCYT (Project CTQ2005-02147).

References

[1] V.S. Mishra, V.V. Mahajani, J.B. Joshi, Ind. Eng. Chem. Res. 34 (1995) 2.
[2] A. Fortuny, C. Bengoa, J. Font, A. Fabregat, J. Hazard. Mater. B 64 (1999) 181.
[3] S. Imamura, I. Fukuda, S. Ishida, Ind. Eng. Chem. Res. 27 (4) (1988) 718.
[4] D. Duprez, F. Delanoë, J. Barbier Jr., P. Isnard, G. Blanchard, Catal. Today 29 (1996) 317.
[5] S.T. Hussain, A. Sayari, F. Larachi, Appl. Catal. B 34 (2001) 1.
[6] M. Abecassis-Wolfovich, M.V. Landau, A. Brenner, M. Herskowitz, Ind. Eng. Chem. Res. 43 (17) (2004) 5089.
[7] F. Larachi, Top. Catal. 33 (1–4) (2005) 109.
[8] J.J. Delgado, J.A. Perez-Omil, J.M. Rodriguez-Izquierdo, M.A. Cauqui, Catal. Commun. 7 (9) (2006) 639.
[9] S. Hamoudi, F. Larachi, G. Cerrella, M. Cassanello, Ind. Eng. Chem. Res. 37 (1998) 3561.
[10] A. Trovarelli, Catalysis by Ceria and Related Materials, Imperial College Press, 2002.
[11] Z.P.G. Masende, B.F.M. Kuster, K.J. Ptasinski, F.J.J.G. Janssen, J.H.Y. Katima, J.C. Schouten, Top. Catal. 33 (1–4) (2005) 87.
[12] J.A. Menezes-Filho, C.R. Paes, C.P. de, J.C. Moreira, P.N. Sarcinelli, D. Mergler, NeuroToxicology 30 (6) (2009) 1207.
[13] S.J. Gregg, K.S.W. Sing, Adsorption, Surface Area and Porosity, Academic Press, London, 1991.
[14] A. Trovarelli, Catal. Rev. Sci. Eng. 38 (4) (1996) 439.
[15] E. Aneggi, M. Boaro, C. Leitenburg, G. Dolcetti, A. Trovarelli, J. Alloys Compd. 408–412 (2006) 1096.
[16] F. Kapteijn, L. Singoredjo, A. Andreini, J.A. Moulijn, Appl. Catal. B: Environ. 3 (2–3) (1994) 173.
[17] Y. Zhang, S. Andersson, M. Muhammed, Appl. Catal. B 6 (1995) 325.
[18] X. Tang, J. Chen, X. Huang, Y. Xu, W. Shen, Appl. Catal. B: Environ. 81 (1–2) (2008) 115.
[19] G. Qi, R.T. Yang, R. Chang, Appl. Catal. B: Environ. 51 (2) (2004) 93.
[20] H. Chen, A. Sayari, A. Adnot, F. Larachi, Appl. Catal. B 32 (2001) 195.